

Tripartite State Characterization via Activated Bipartite Entanglement

L. G. E. Arruda,¹ W. F. Balthazar,^{2,3} M. V. Moreira,¹ M. H. M. Passos,⁴ J. A. O. Huguenin,^{5,3} and M. C. de Oliveira^{1,*}

¹*Instituto de Física Gleb Wataghin, Universidade de Campinas, 13083-970, Campinas, SP, Brazil*

²*Instituto Federal de Educação, Ciência e Tecnologia do Rio de Janeiro - IFRJ, Volta Redonda, RJ, Brazil*

³*Programa de Pós-graduação em Física, Instituto de Física, Universidade Federal Fluminense, Niterói, RJ, Brazil*

⁴*ICFO—Institut de Ciències Fotoniques, the Barcelona Institute of Science and Technology, 08860 Castelldefels (Barcelona), Spain*

⁵*Instituto de Ciências Exatas, Universidade Federal Fluminense, Volta Redonda, RJ, Brazil*

(Dated: March 15, 2022)

We propose a procedure to identify and classify genuine tripartite entanglement in pure 3-qubit states via the Activated Bipartite Entanglement (ABE), which is defined here as the difference between the Entanglement of Assistance and the Entanglement of Formation. We show that for pure states belonging to one of the two inequivalent classes of genuine tripartite entanglement, i.e., GHZ or W states, the ABE is always greater than zero. For separable and biseparable states it is always null. In addition, our approach is capable to distinguish between genuine tripartite entangled states, those belonging to the GHZ class from those belonging to the W class. We also present an experimental proposal, by using linear optical circuits and internal degrees of freedom of a single photon, to measure the ABE and to verify the characterization via activated entanglement. The circuit simulation shows an excellent agreement with theoretical prediction for a wide class of GHZ and W states.

After decades of theoretical and experimental research, entanglement has gained the status of fundamental non-local resource, necessary to accomplish informational tasks in a more efficient way than in classical systems. While bipartite entanglement is well understood and properly quantified for arbitrarily mixed states, for both discrete [1] and continuous variable [2], quantitative and qualitative characterization of multipartite entanglement has been challenging [3].

In this paper, we propose a procedure to quantitatively distinguish pure 3-qubit states possessing genuine tripartite entanglement from biseparable and separable states by means of the Activated Bipartite Entanglement (ABE), which quantifies the amount of entanglement shared by the combined system ABC that can be exclusively localised within the subsystem AB by local operations on subsystem C . The ABE turns out to be the difference between two dual entanglement measures: the Entanglement of Assistance (EoA) [4] and the Entanglement of Formation (EoF) [5]. Moreover, it allows to distinguish among the genuine tripartite entangled states, those belonging to the GHZ-class from those belonging to the W-class. This difference between the posterior and the anterior amount of entanglement localised within AB by means of local operations on C also enables a clear ordering of states in a parameter map. Through the Generalized Schmidt Decomposition [6], for one independent parameter (1-parameter GHZ-type) and for two independent parameters (2-parameter W-type) states [7], we obtain exact analytical results, shedding light on how pure tripartite states are distributed in a parametric space defined by three parametric functions given by the ABE, its upper bound and the dependent Schmidt coefficient.

Furthermore, we present an experimental proposal for the generation of 1-parameter GHZ and 2-parameter W states employing linear optics. Linear optical circuits are very precise and an excellent test bed for entanglement analysis [8–11]. Besides, internal degrees of freedom of twin-photons were explored for study of multipartite states [12]. They have been used, for instance, for the implementation of the sudden death

entanglement induced by environments emulated by linear transformations of polarization of twin-photons [9], by polarization mode dispersion [10] and by an all-optical local CNOT [11]. Internal degrees of freedom of twin-photons were also explored for preparation and geometry study of GHZ states [12, 13]. By using path, polarization, and transverse mode degrees of freedom of single photons, it was previously proposed a full linear optical circuit to prepare tripartite GHZ state [14, 15]. Here, also using these three degrees of freedom we propose an experimental detection of ABE for 1-parameter GHZ and 2-parameter W states.

The definition of the EoA is motivated by the situation in which three parties spatially separated, ABC (A , B and C stand for Alice, Bob and Charlie, respectively), share many copies of a pure tripartite entangled state given by $\rho_{ABC} = |\psi_{ABC}\rangle\langle\psi_{ABC}|$, and AB would like to use their subsystems to perform some particular task. However, the reduced state $\rho_{AB} = \text{Tr}_C[\rho_{ABC}]$ might not be very pure nor sufficiently entangled for this purpose. However, C can effectively help them by remotely transforming the available resource through appropriate local projective measurements in his subsystem. This procedure concentrates the initial tripartite entanglement in a new set of bipartite copies shared by AB . The more accurately chosen is the measurement basis, the higher is the concentrated entanglement. The rate that AB can convert their copies (regardless of C 's assistance) into singlets to perform their task is given by [16]

$$\bar{S}(\varepsilon) = \sum_i p_i S(\rho_A^i) = - \sum_i p_i \text{Tr}(\rho_A^i \log \rho_A^i), \quad (1)$$

where $\varepsilon = \{p_i, \rho_{AB}^i\}$ represents the ensemble made of pure states $\rho_{AB}^i = |\psi_{AB}^i\rangle\langle\psi_{AB}^i|$ with classical probabilities p_i . The EoA is defined as

$$E_A(\rho_{AB}) = \max_{\varepsilon} \bar{S}(\varepsilon) = \max_{\{p_i, \rho_{AB}^i\}} \sum_i p_i S(\rho_A^i), \quad (2)$$

i.e., it is the maximization of the conversion rate given by Eq. (1) over all convex decomposition of ρ_{AB} into pure

states, that is, over all ensembles ε for which $\rho_{AB} = \sum_i p_i |\psi_{AB}^i\rangle\langle\psi_{AB}^i|$. The EoF is the dual measure of the EoA in the sense that it is defined as the minimum value of the average entropy $\bar{S}(\varepsilon)$ over all possible pure state decomposition of ρ_{AB} [5],

$$E_F(\rho_{AB}) = \min_{\varepsilon} \bar{S}(\varepsilon) = \min_{\{p_i, \rho_{AB}^i\}} \sum_i p_i S(\rho_A^i). \quad (3)$$

Note that the EoF captures the amount of entanglement shared by the pair AB , independently of action on subsystem C . On the other hand, the EoA captures the total amount of entanglement that is localised within AB after the assistance of C . Nevertheless, the EoA does not distinguish whether ρ_{AB} was previously entangled or not.

To account exclusively for the extra entanglement that can be concentrated in the subsystem AB through local projective measurements on C , the ABE is defined as the maximal difference between the average entropy, $\bar{S}(\varepsilon)$, of the reduced state ρ_A , anterior and posterior the action on C ,

$$\begin{aligned} \Delta_E(\rho_{AB}) &\equiv \max_{\varepsilon} [\bar{S}(\varepsilon_p) - \bar{S}(\varepsilon_a)] \\ &= \max_{\varepsilon_p} \bar{S}(\varepsilon_p) - \min_{\varepsilon_a} \bar{S}(\varepsilon_a), \end{aligned} \quad (4)$$

where ε_a and ε_p represent the anterior (prior operation on C) and posterior (after operation on C) ensembles of pure state decomposition of $\rho_{AB} = \text{Tr}_C \rho_{ABC}$ and $\rho_{AB}^p \equiv \text{Tr}_C [\sum_i \Pi_i \rho_{ABC} \Pi_i]$, with $\Pi_i = \mathbf{1}_A \otimes \mathbf{1}_B \otimes |i\rangle\langle i|$ ($i = 1, 2$) being the two projectors of C . Therefore, the ABE given by Eq. (4) can be expressed as the difference between the EoA and the EoF as given by Eqs. (2) and (3),

$$\Delta_E(\rho_{AB}) = E_A(\rho_{AB}) - E_F(\rho_{AB}). \quad (5)$$

For many copies of a state ρ_{ABC} , the ABE quantifies the rate of maximally entangled bipartite states that are successfully activated. In other words, $E_F(\rho_{AB})$ measures the amount of entanglement already existing within AB before the assistance of C , while $\Delta_E(\rho_{AB})$ represents exclusively the extra amount of entanglement added to the preexisting one, after the assistance.

To conduct a proper analysis of the behavior of arbitrary pure tripartite states in terms of ABE, let us consider its lower and upper bounds,

$$0 \leq \Delta_E(\rho_{AB}) \leq \Delta S, \quad (6)$$

where $\Delta S = S(\rho_{AB}) - |S(\rho_A) - S(\rho_B)|$.

First, it is important to note that the lower bound on the EoA, $E_F(\rho_{AB}) \leq E_A(\rho_{AB})$, is implicit, and $\Delta_E(\rho_{AB}) = 0$, i.e., $E_A(\rho_{AB}) = E_F(\rho_{AB})$ only for biseparable and separable pure tripartite states. The physical meaning for the nullity of ABE is the following: there is no local measurement made on C that is capable to concentrate any extra amount of entanglement between AB , besides the already existing (the $E_F(\rho_{AB})$), if the combined system ABC shares non-genuine tripartite entanglement. The fact that $\Delta_E(\rho_{AB}) = 0$

for all biseparable and separable tripartite states can be easily checked, noting that ΔS is always equals to zero for these states. On the other hand, states with genuine tripartite entanglement, such as GHZ-type and W-type, show $\Delta_E(\rho_{AB}) > 0$. Thus, $\Delta_E(\rho_{AB})$ can be used to test if a pure 3-qubit state presents genuine tripartite entanglement or not. More important, $\Delta_E(\rho_{AB})$ can be used to retrieve information about the type of genuine tripartite entanglement (GHZ or W) a state with $\Delta_E(\rho_{AB}) > 0$ possesses.

To observe the bounds for tripartite entanglement, we must be able to prepare a wide class of 3-qubit GHZ-type and W-type states. Here we present an experimental proposal based on the utilisation of internal degrees of freedom of light [14, 15] associated with single photon source produced by SPDC [12]. In particular, we use three degrees of freedom of a single photon to codify the qubits, namely the propagation path (p), the polarization (P), and the transverse modes (M). Our tripartite state is described by $|pPM\rangle$. We codify subsystem A in the polarization degree of freedom ($|H\rangle \equiv |0\rangle, |V\rangle \equiv |1\rangle$), subsystem B in the first order of HG modes ($|HG_{10}\rangle = |h\rangle \equiv |0\rangle, |HG_{01}\rangle = |v\rangle \equiv |1\rangle$), and subsystem C in path degree of freedom ($|up\rangle = |u\rangle \equiv |0\rangle, |down\rangle = |d\rangle \equiv |1\rangle$) [15]. We define the order of qubits as $|C\rangle \otimes |A\rangle \otimes |B\rangle$.

The preparation of tripartite states utilising the three internal degrees of freedom of a photon follows the proposal of Ref. [15]. Polarized single photons can be prepared with h/v transverse modes and have their path controlled. Then, a general tripartite state can be prepared. Let us show the optical circuits and their simulation for GHZ and W states.

The schematic optical circuit for preparation of a single photon in GHZ-type state defined in Eq. (9) is presented in Fig. 1. A Spontaneous Parametric Down Conversion (SPDC) source composed by a Laser of frequency ω_p pumping a non-linear crystal (NLC) produces twin photons – the Signal with frequency ω_s is used for GHZ preparation and the Idler with frequency ω_i is used to trigger the measurement apparatus. Naturally, the phase matching condition $\omega_p = \omega_s + \omega_i$ is satisfied. The Signal passes through a S-Wave Plate (SWP) in order to prepare radial polarization, that corresponds to the spin-orbit entangled state of the system AB . In the first Polarized Beam Splitter (PBS₁), a polarization projective measurement is performed producing the state $|\Psi_1\rangle = |Hh\rangle \equiv |00\rangle_{AB}$. This is a simple and very efficient way to prepare the initial state. A path qubit can be prepared by a variable Beam Splitter that can be performed by the Half Wave Plate (HWP) with its fast axis making an angle of θ with the horizontal plane and a PBS. The HWP _{θ} transforms the polarization producing the following state

$$|\Psi_2\rangle = |h\rangle \otimes [\cos(2\theta)|H\rangle + \sin(2\theta)|V\rangle]. \quad (7)$$

The PBS₂ projects H-polarization in path u and V-polarization in path d . Then, we have a tripartite state prepared as

$$|\Psi_3\rangle = \cos(2\theta)|uHh\rangle + \sin(2\theta)|dVh\rangle. \quad (8)$$

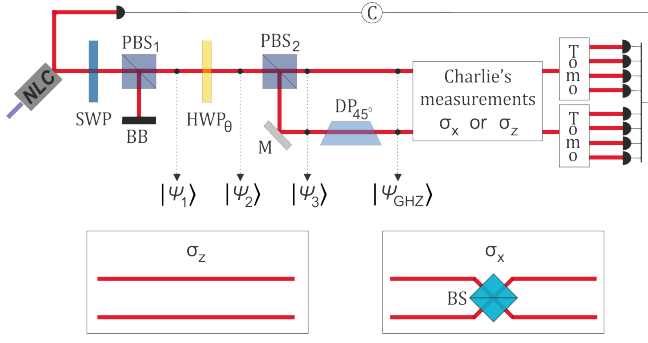


FIG. 1. Experimental setup for GHZ-type states. NLC: non linear crystal, SWP: S-wave plate to produce spin-orbit non-separable modes, PBS: Polarized Beam Splitter, HWP_θ : half wave plate with its fast axis making an angle of θ with the horizontal plane, DP_{45° : Dove Prism with its base rotated 45° with respect the horizontal plane, TOMO: tomography circuit for spin-orbit states as proposed in Ref.[17]. The tomography outputs in both paths are detected by photodetectors that are triggered by coincidence with the detection of Idler. BS: 50/50 non polarized Beam Splitter.

Finally, the Dove Prism (DP) performs the transformation of the transverse mode $|h\rangle \rightarrow |v\rangle$ in the path d , and the Signal photon becomes the state

$$\begin{aligned} |\Psi_{GHZ}\rangle &= \cos(2\theta) |uHh\rangle + \sin(2\theta) |dVv\rangle \\ &\equiv \lambda_1 |000\rangle + \lambda_2 |111\rangle, \end{aligned} \quad (9)$$

where $\lambda_1 = \cos(2\theta)$ and $\lambda_2 = \sin(2\theta)$, with $\lambda_2 = \sqrt{1 - \lambda_1^2}$. The preparation of 1-parameter GHZ state is complete. Let us discuss the measurement. At the end of each path we have a spin-orbit state tomography circuit as presented in [17]. With the tomography circuit we reconstruct the reduced density matrix ρ_{AB} . However, before the tomography C needs to perform σ_x and σ_z measurements, since these are the bases that respectively optimize Eqs. (2) and (3) in the case of 1-parameter GHZ states. For σ_z , both paths are free and the click in the paths u or d gives the outcome 0 or 1 for this measure. For σ_x , path u and d are sent to a Beam Splitter (BS) [14] and the output coming from it goes to tomography circuit.

We simulate the preparation and measurement of 1-parameter GHZ states by using Jones Matrix formalism [18]. Our experimental proposal is designed to give as output the reduced density matrix ρ_{AB} of spin-orbit states multiplied by the corresponding weight that depends on λ_1 and λ_2 . The matrix obtained is used to calculate the difference: $E_A(\rho_{AB}) - E_F(\rho_{AB})$. In order to emulate experimental errors, we introduce in the simulation an error of $\pm 1^\circ$ in the angle θ of the HWP that defines the parameters λ_1 and λ_2 .

Analytical results show that states of this kind have $E_F(\rho_{AB}) = 0$ and $E_A(\rho_{AB}) = S(\rho_{AB}) = S(\rho_A) = S(\rho_B) = S(\rho_C) = -\lambda_1^2 \log_2(\lambda_1^2) - \lambda_2^2 \log_2(\lambda_2^2)$, which implies that

$$\Delta_E(\rho_{AB}) = E_A(\rho_{AB}) = S(\rho_{AB}). \quad (10)$$

This implies that every 1-parameter GHZ state saturates the upper bound given in Eq. (6), maximizing the amount of ex-

tra entanglement localised within AB via local operations on C . In Fig. 2, the saturation given by Eq. (10) is represented in a parametric space defined by the one variable parametric functions: $E_A(\rho_{AB})$, $S(\rho_{AB})$ and $\lambda_2 = \sqrt{1 - \lambda_1^2}$. The blue curved line in Fig. 2-top represents the 1-parameter GHZ states given by Eq. (9). The red squares are the outcomes of the optical circuit simulation, whose results are in a remarkable agreement with theoretical expectation. Irrespective of the value assumed by λ_1 , the optimal measurement basis that maximizes the extra amount of entanglement between AB is spanned by the eigenvectors of Pauli's σ_z operator. The basis formed by the eigenvectors of Pauli's σ_x is the worst basis that C can choose to perform his measurements, the one where $E_A(\rho_{AB}) = E_F(\rho_{AB})$ and no extra entanglement is activated. Since the entanglement between any bi-partition is zero before operations on C and, after that, is equal to the total amount of entanglement shared initially by the trio ABC , the assistance is a full assistance and the saturation given by Eq. (10) represents a characteristic only fulfilled by 1-parameter GHZ states.

States given by Eq. (9) come from the Generalized Schmidt Decomposition [6, 7],

$$|\psi\rangle = \lambda_0 |000\rangle + \lambda_1 e^{i\phi} |100\rangle + \lambda_2 |101\rangle + \lambda_3 |110\rangle + \lambda_4 |111\rangle, \quad (11)$$

where $\lambda_i \geq 0$, $\sum_i \lambda_i^2 = 1$ and $0 \leq \phi \leq \pi$. These states describe arbitrary pure tripartite states with 5 independent parameters.

Through the states given by Eq. (11), it is possible to analyse the ABE for the W states by means of two different decompositions,

$$|\psi_{W2}\rangle = \lambda_0 |100\rangle + \lambda_3 |010\rangle + \lambda_2 |001\rangle, \quad (12)$$

$$|\psi_{W3}\rangle = \lambda_0 |000\rangle + \lambda_1 |100\rangle + \lambda_2 |101\rangle + \lambda_3 |110\rangle, \quad (13)$$

where the coefficients in both must satisfy the constraints $\lambda_i \geq 0$ and $\sum_i \lambda_i^2 = 1$. The states given by 2 independent parameters (2-parameter W states given by Eq. (12)) are particular cases of general W states given by 3 independent parameters (3-parameter W states) making $\lambda_1 = 0$ in Eq. (13) and applying a BIT-FLIP operation on the first qubit of each product state of the remaining superposition.

Figure 3 presents the schematic optical circuit for preparation and measurements of 2-parameter W states. The circuit is the same one as for GHZ-type up to the point depicted in the Fig. 3 by the state $|\Psi_3\rangle$, which is given by Eq. (8). Here, α is the angle of the first HWP for path preparation. A photon in the path d passes through a HWP_{45° and transforms its polarization as $|V\rangle \rightarrow |H\rangle$ and this part of the state is in accordance of the first term of Eq. (12), $\lambda_0 |100\rangle$, where $\lambda_0 = \sin(2\alpha)$ and $|100\rangle \equiv |dHh\rangle$. The other two terms are associate to path u , and we can write $|0\rangle_C \otimes (\lambda_3 |10\rangle + \lambda_2 |01\rangle)$. The terms in parentheses are an unbalanced entangled state in the spin-orbit degree of freedom of light with weights λ_2 and λ_3 . It can be prepared by a C-NOT, using polarization as control qubit. The

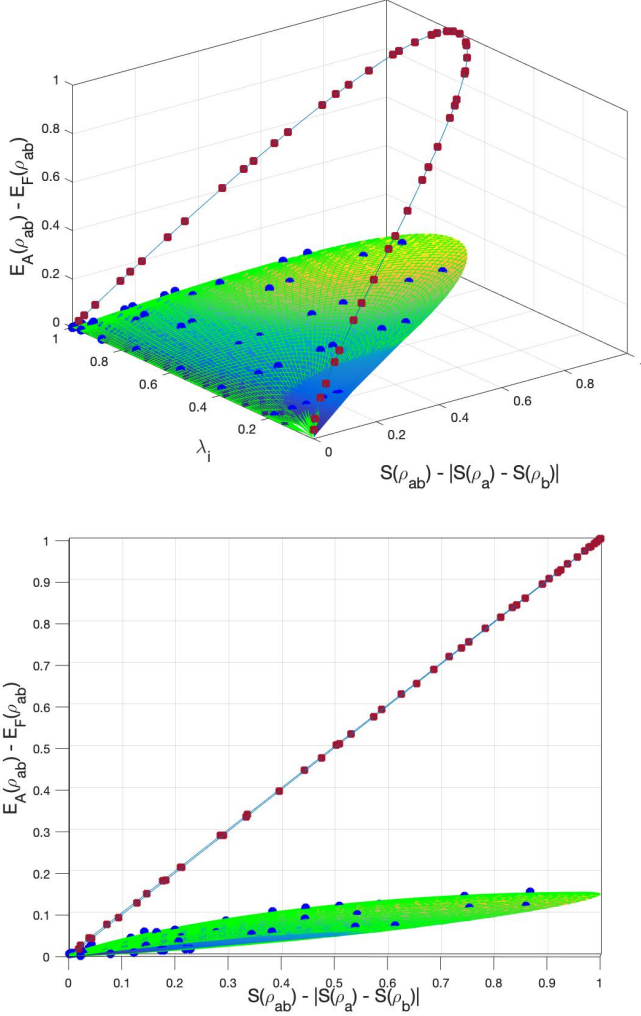


FIG. 2. Top: Parametric curve and parametric surface for both, 1-parameter GHZ and 2-parameter W states, respectively. Bottom: $E_F(\rho_{AB}) \times S(\rho_{AB}) - |S(\rho_A) - S(\rho_B)|$. The red squares and the dark-blue dots are the outcomes stemming optical circuit simulation.

HWP $_{\beta}$ will transform

$$\cos(2\alpha) |Hh\rangle \rightarrow \cos(2\alpha) [\cos(2\beta) |H\rangle + \sin(2\beta) |V\rangle]. \quad (14)$$

The V-polarization is reflected by PBS $_3$ and is deviated towards PBS $_4$. The H-polarization is transmitted in PBS $_3$, passes through a DP that transforms the transverse mode as $|h\rangle \rightarrow |v\rangle$ and is transmitted by PBS $_4$ where is aligned with the other arm in the path u . Then, finally, we have

$$|\Psi_W\rangle = \sin(2\alpha) |dHh\rangle + \cos(2\alpha) \cos(2\beta) |uHv\rangle + \cos(2\alpha) \sin(2\beta) |uVh\rangle. \quad (15)$$

Taking into account our codification and by comparing with Eq. (12), we identify $\lambda_3 = \cos(2\alpha) \cos(2\beta)$ and $\lambda_2 = \cos(2\alpha) \sin(2\beta)$. Here, the preparation of W-type state is complete. The measurement circuit is the same used for GHZ-

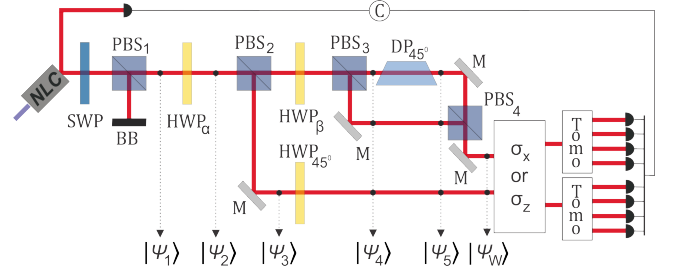


FIG. 3. Experimental setup for W-type state preparation. NLC: non linear crystal, SWP: S-wave plate to produce spin-orbit nonseparable modes, PBS: Polarized Beam Splitter, HWP $_{\phi}$: half wave plate with its fast axis making an angle of $\phi = \alpha, \beta, 45^\circ$ with the horizontal plane, DP $_{45^\circ}$: Dove Prism with its base rotated 45° with respect the horizontal plane, TOMO: tomography circuit for spin-orbit states as proposed in Ref. [17]. The tomography outputs in both paths are detected by photcounters detectors that are triggered by coincidence with the detection of Idler.

type states.

The EoF of W-vectors given by Eqs. (12) and (13) is not equal to zero in general, depending solely on the values of the independent parameters. Analytical result for the EoF of the 2-parameter W states is given by the following expression

$$E_F(\rho_{AB}^{W2}) = 1 + \frac{\mathcal{F}(1 - \sqrt{1 - 4\lambda_3^2 \cdot \lambda_0^2})}{2} + \frac{\mathcal{F}(1 + \sqrt{1 - 4\lambda_3^2 \cdot \lambda_0^2})}{2}, \quad (16)$$

where $\mathcal{F}(x) = -x \log_2(x)$. The analytical result for the EoA of 2-parameter W states gives

$$E_A(\rho_{AB}^{W2}) = -\mathcal{F}(\lambda_0^2 + \lambda_3^2) + \mathcal{F}(\lambda_0^2) + \mathcal{F}(\lambda_3^2), \quad (17)$$

and for the upper bound ΔS^{W2} as given by Eq. (6),

$$\Delta S^{W2} = \mathcal{F}(\lambda_0^2 + \lambda_3^2) + \mathcal{F}(1 - \lambda_0^2 - \lambda_3^2) - |\mathcal{F}(\lambda_0^2) + \mathcal{F}(1 - \lambda_0^2) - \mathcal{F}(\lambda_3^2) - \mathcal{F}(1 - \lambda_3^2)|. \quad (18)$$

With the help of Eqs. (16), (17) and (18), it is possible to see that not only 2-parameter W states given by Eq. (12) but also general W states given by Eq. (13), are contained in the parametric surface depicted in Fig. 2 and defined by the two variables (λ_0, λ_3) parametric functions: $\Delta_E(\rho_{AB}^{W2}) = E_A(\rho_{AB}^{W2}) - E_F(\rho_{AB}^{W2})$, ΔS^{W2} and $\lambda_2 = \sqrt{1 - \lambda_0^2 - \lambda_3^2}$. The surface illustrated in Fig. 2-top represents the general W-vector world. This means that every W state must necessarily lie over the parametric surface, and any state with $\Delta_E(\rho_{AB}) > 0$ that is not on this surface must necessarily be a GHZ state. The dark-blue dots represent the outcomes obtained from the optical circuit simulation. This finding, which is obtained analytically, redefines the upper bound on the total extra entanglement which can be concentrated in AB by local operations in C for general W states:

$$0 \leq \Delta_E(\rho_{AB}^{W\text{-type}}) \lesssim 0.15. \quad (19)$$

Since the upper bound given by Eq. (19) is a limiting value for general W states, every state with $\Delta_E(\rho_{AB}) > 0.15$ is necessarily a GHZ state. However, note that this upper bound on W states is not a lower bound on GHZ states. The basis that maximizes and minimizes the average entropy for W states are the other way around compared to the 1-parameter GHZ states, which means that, for W states, measuring in the σ_z basis maximizes the average entropy while measuring in the σ_x basis minimizes it.

Last but not least, we perform ABE analysis considering randomly generated arbitrary pure tripartite states obeying the Haar measure. The optimizations in Eqs. (2) and (3) were numerically solved. In Fig. 4, we plot 8×10^4 of these states depicted by the background light-blue dots. As can be observed, these dots spread almost all over the allowed area defined by the ABE's lower and upper bounds. Numerical analysis of the 1-parameter GHZ-vectors, the 2 and 3-parameter W-vectors and the arbitrary vectors given by Eqs. (9), (12), (13) and (11), respectively, are included. In each case the independent parameters were randomly chosen. The 1-parameter GHZ-vectors are represented in Fig. 4 by 1×10^3 green dots along the straight line $\Delta_E(\rho_{AB}) = \Delta S$ (the saturation line). The 2 and 3-parameter W-vectors are represented by the 2×10^3 orange dots situated in a limited region representing the W parametric surface shading the 2-dimensional parametric plane defined by the axes $\Delta_E(\rho_{AB})$ and ΔS (see Fig. 2-bottom for comparison). The maximum value attained by the ABE for these states is $\Delta_E(\rho_{AB}) \approx 0.15$, which is in accordance with the analytical results. The sparse red dots scattered along the same allowed area represent 1×10^2 four independent parameters arbitrary pure tripartite states given by Eq. (11) (for simplicity, we neglect the phase parameter: $\phi = 0$). Calculations of the rank of the reduced density matrices of each individual subsystem ($r(\rho_k)$, $k = A, B, C$) show that all the states for which $\Delta_E(\rho_{AB}) > 0$, present $r(\rho_A) = r(\rho_B) = r(\rho_C) = 2$, which is a *sine qua non* condition to identify true tripartite entangled states. Therefore, all the states in Fig. 4 with $\Delta_E(\rho_{AB}) > 0$ are necessarily GHZ or W states. On the other hand, calculations show that the orange dots formed by 2 and 3-parameter W-vectors possess the 3-tangle [19] equals to zero, which is a characteristic of W states [20]. Calculations of the 3-tangle for the arbitrary states show that the light-blue and red dots that present vanishing 3-tangle values are precisely located at the same region representing the W-parametric surface. Thus, the arbitrary pure tripartite states located behind the 2 and 3-parameter W-vectors in Fig. 4 are all W states. In the same figure, we highlight the ordinary W-state with $\lambda_0 = \lambda_3 = 1/\sqrt{3}$, depicted as the big orange dot at coordinates $(\Delta_E(\rho_{AB}^W), \Delta S^W) = (0.11, 0.9183)$. The light-blue dots above the W-region (and here we include the green 1-parameter GHZ-vectors) have tangle greater than zero, which is a characteristic trait only fulfilled by the GZH-states. Therefore, we conclude that all the states above the W-region are GHZ states. The ordinary GHZ state given by $\lambda_1 = 1/\sqrt{2}$ in Eq. 9, is represented in Fig. 4 by the big green dot whose coordinates are (1,1). This state possesses the greater value

that ABE can assume. The dots at the origin correspond to all biseparable and separable states for which the ranks are in agreement with the expected [20]: for biseparable states, one of them is equal to 1 and for completely separable states the three 3-tangle is equal to 1.

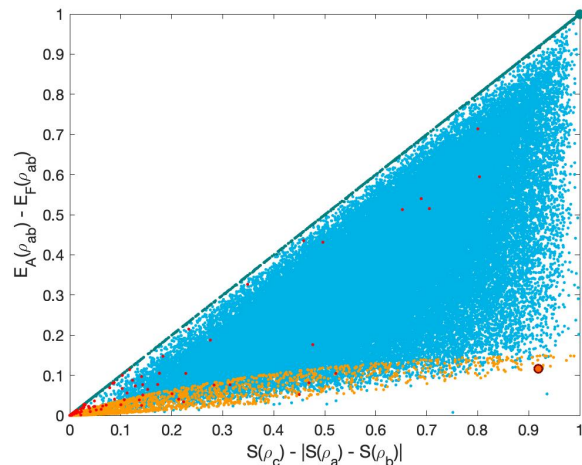


FIG. 4. The (numerically solved) Activated Bipartite Entanglement plotted against its upper bound. The dots in light-blue represent a total of 8×10^4 randomly generated pure tripartite states satisfying the Haar measure. The dots in green over the straight line $E_A(\rho_{AB}) - E_F(\rho_{AB}) = S(\rho_{AB}) - |S(\rho_A) - S(\rho_B)|$ represent a total of 1×10^3 1-parameter GHZ-vectors. The dots in orange represent a total of 2×10^3 W-vectors with half of them given by the 3-parameter W-type decomposition and the other half formed by the 2-parameter W-type decomposition. The dots in red represent a total of 1×10^2 arbitrary states given by Eq. (11). The two big dots at coordinates (1,1) (green) and (0.11,0.9183) (orange) are, respectively, the ordinary GHZ and W states.

We proposed a procedure to determine when pure 3-qubit states present genuine tripartite entanglement via the Activated Bipartite Entanglement (ABE). This approach reveals that when the states present genuine tripartite entanglement, the ABE is necessarily greater than zero and, otherwise, it is equal to zero. Moreover, this approach is capable to distinguish between genuine tripartite entangled states, those belonging to the GHZ class from those belonging to the W class. We should remark that, as we have only considered projective operations on C , it resulted in the ABE being defined in terms of the EoA and EoF. We could extend the formalism to general POVM, and it would give similar results in terms of the Localizable Entanglement [21], instead. However, this approach would be more difficult to calculate and to experimentally implement. Besides, it would not bring any additional insight. We also presented an experimental proposal to measure ABE by using non linear circuit to prepare tripartite states codifying qubits in internal degrees of freedom of a single photon. The optical circuits was designed to prepare GHZ and W states and perform all measurements. Simulations of the optical circuits show an excellent agreement with theory.

We would like to thank financial support from the Brazil-

ian funding agencies Conselho Nacional de Desenvolvimento Científico e Tecnológico (CNPq), through the Brazilian National Institute for Science and Technology of Quantum Information (INCT-IQ), Fundação Carlos Chagas Filho de Amparo à Pesquisa do Estado do Rio de Janeiro (FAPERJ), Coordenação de Aperfeiçoamento de Pessoal de Nível Superior (CAPES). L.G.E.A. would like to thank Felipe F. Fanchini for the computational support provided.

* marcos@ifi.unicamp.br

- [1] F. E. Steinhoff and M. C. de Oliveira, *Quantum Information and Computation* **10**, 525 (2010).
- [2] M. C. de Oliveira, *Phys. Rev. A* **72**, 012317 (2005).
- [3] T. R. de Oliveira, G. Rigolin, M. C. de Oliveira, and E. Miranda, *Phys. Rev. Lett.* **97**, 170401 (2006).
- [4] D. P. DiVincenzo, C. A. Fuchs, H. Mabuchi, J. A. Smolin, A. Thapliyal, and A. Uhlmann, in *Quantum Computing and Quantum Communications*, edited by C. P. Williams (Springer, 1998) pp. 247–257.
- [5] W. K. Wootters, *Physical Review Letters* **80**, 2245 (1998).
- [6] A. Acín, A. Andrianov, L. Costa, E. Jané, J. Latorre, and R. Tarrach, *Physical Review Letters* **85**, 1560 (2000).
- [7] A. Acín, D. Bruß, M. Lewenstein, and A. Sanpera, *Physical Review Letters* **87**, 040401 (2001).
- [8] J.-W. Pan, Z.-B. Chen, C.-Y. Lu, H. Weinfurter, A. Zeilinger, and M. Żukowski, *Reviews of Modern Physics* **84**, 777 (2012).
- [9] M. P. Almeida, F. de Melo, M. Hor-Meyll, A. Salles, S. P. Walborn, P. H. S. Ribeiro, and L. Davidovich, *Science* **316**, 579 (2007), <https://www.science.org/doi/pdf/10.1126/science.1139892>.
- [10] C. Antonelli, M. Shtauf, and M. Brodsky, *Physical review letters* **106**, 080404 (2011).
- [11] A. Singh, S. Pradyumna, A. R. P. Rau, and U. Sinha, *J. Opt. Soc. Am. B* **34**, 681 (2017).
- [12] G. Carvacho, F. Graffitti, V. D’Ambrosio, B. C. Hiesmayr, and F. Sciarrino, *Sci. Rep.* **7**, 13265 (2017).
- [13] X.-L. Wang, Y.-H. Luo, H.-L. Huang, M.-C. Chen, Z.-E. Su, C. Liu, C. Chen, W. Li, Y.-Q. Fang, X. Jiang, J. Zhang, L. Li, N.-L. Liu, C.-Y. Lu, and J.-W. Pan, *Phys. Rev. Lett.* **120**, 260502 (2018).
- [14] W. F. Balthazar, C. E. R. Souza, D. P. Caetano, E. F. G. ao, J. A. O. Huguenin, and A. Z. Khoury, *Opt. Lett.* **41**, 5797 (2016).
- [15] W. F. Balthazar and J. A. O. Huguenin, *J. Opt. Soc. Am. B* **33**, 1649 (2016).
- [16] C. H. Bennett, H. J. Bernstein, S. Popescu, and B. Schumacher, *Physical Review A* **53**, 2046 (1996).
- [17] W. F. Balthazar, D. G. Braga, V. S. Lamego, M. H. M. Passos, and J. A. O. Huguenin, *Phys. Rev. A* **103**, 022411 (2021).
- [18] R. C. Jones, *J. Opt. Soc. Am.* **31**, 488 (1941).
- [19] V. Coffman, J. Kundu, and W. K. Wootters, *Phys. Rev. A* **61**, 052306 (2000).
- [20] W. Dür, G. Vidal, and J. I. Cirac, *Phys. Rev. A* **62**, 062314 (2000).
- [21] M. Popp, F. Verstraete, M. A. Martín-Delgado, and J. I. Cirac, *Phys. Rev. A* **71**, 042306 (2005).